Hydrology Research

Hydrology Research Vol 55 No 3, 380 doi: 10.2166/nh.2024.178

Temporal dynamics of water level and water sources analyses of karst tidal springs in Guilin, China

Jie Ma[a,b,c], Shilong Zhu[b,c], Xiaomei Wei[d], Yongli Guo[b,c], Jianhua Cao[b,c] and Fen Huang[b,c,*]

[a] Environmental Science and Engineering, Guilin University of Technology, Guilin 541006, China
[b] Institute of Karst Geology, CAGS/ Key Laboratory of Karst Dynamics, MNR & Guangxi /International Research Center on Karst, UNESCO, Guilin, Guangxi 541004, China
[c] Pingguo Guangxi, Karst Ecosystem, National Observation and Research Station, Pingguo, Guangxi 531406, China
[d] Guangxi Nonferrous Survey Surveyhina, Nanning, Guangxi 530031, China
*Corresponding author. E-mail: huangfen@mail.cgs.gov.cn

FH, 0000-0002-8833-873X

ABSTRACT

The hydrological dynamics and sources of karst tidal springs are difficult to capture and quantify due to fluctuations in their flow velocity. In this study, the Laolongshui (LLS) karst tidal spring in the Maocun underground river basin of Guilin City was taken as an example, with a 2-year continuous monitoring of the electrical conductivity, and water level, as well as water chemical analysis. The results showed the following: (1) discovered the variation pattern of LLS water level in different seasons, the water level fluctuates regularly on a daily scale, with a rise and fall time of 43.6 min after heavy rainfall in the rainy season, while in the dry season, it lasts for about 74–80 h. (2) Four peaks were extracted from the frequency distribution of electrical conductivity, representing the response of springwater under different rainfall conditions. (3) The annual average frequencies of the occurrence of P1, P2, P3, and P4 in terms of time are 53.82, 39.29, 6.18, and 0.72%, respectively. The results provide a new method for analyzing groundwater's source and dynamic changes in karst areas.

Key words: conductance frequency distribution, diurnal variation, groundwater source

HIGHLIGHTS

- Two years of automatic continuous monitoring illustrated the water level fluctuation of a typical karst tidal spring.
- Explaining the forming mechanism of karst tidal springs.
- The frequency distribution of conductivity quantified the source of karst water.
- Providing a fast and low-cost new method for identifying karst water sources.
- Enriching groundwater investigation methods and understanding of underground structures.

1. INTRODUCTION

Globally, the exposed area of carbonate rocks covers about 12% of the land area (Cao *et al.* 2003), and about 25% of the world's population depends wholly or partially on drinking water from karst aquifers (Dar *et al.* 2014). In many regions, karst water is the main source of drinking water (Vasić *et al.* 2019; Moldovan *et al.* 2020). Spring refers to the phenomenon of groundwater gushing out from the surface at the intersection of an aquifer or aquifer channel with the ground (Zhou & Li 2022), while a karst spring refers to a spring formed in karst areas due to the dissolution of soluble salt rocks, where surface water quickly emerges in the form of a spring after infiltrating the cave (Wang *et al.* 2008), and their water sources reflect the geological background of the spring basin and the surface and groundwater processes. The media of aquifers in karst areas show heterogeneity (Goldscheider & Drew. 2007), and due to the complexity of the medium composition, fracture development, and uneven distribution (Hartmann *et al.* 2014; Medici *et al.* 2023), the karst water migration law is more complex than that of pore water (Zhang *et al.* 2019). In addition, the complex physical environment and water movement patterns in karst areas also increase the difficulty of identifying the source of karst springwater (Palmer. 2010). The source of springwater

recharge is mainly atmospheric precipitation, but the depth, recharge direction, and recharge size of different spring groups are not clear (Hou 2019), so clarifying the sources and dynamics of karst springwater is still a difficult problem.

Affected by special hydrogeological conditions, the hydrodynamic process and material cycle process in the karst basin of southwestern China are complex, and it is difficult to analyze the hydrodynamic process in the area by using a single water parameter. At present, researchers mainly use water chemistry and electrical conductivity to identify the source of springwater components. Electrical conductivity is an important indicator in water quality analysis, often used to evaluate soil salinization and groundwater quality (Yu *et al.* 2020) and also used to indirectly estimate the total concentration of ionic components in water (Chen 2000). The electrical conductivity of water is mainly determined by the type of ions dissolved in water, their concentration, and the water temperature (Gao *et al.* 2006). Water chemistry data are often used to characterize the internal hydrodynamic characteristics of karst aquifers (Richieri *et al.* 2023), using natural components or indicators dissolved in water as natural tracers (Jiang *et al.* 2015). Bakalowicz (Bakalowicz 1979) argued that different patterns of conductance frequency distribution (CFD) in karst springs reflect the geochemical movement of different water masses through the aquifer, and the average conductance of a single water mass or type depends on its source and residence time. The so-called frequency distribution is to divide data into several groups according to certain rules. The number of data falling within each group is called frequency, and the ratio of the frequency of each group to the total number of data is called frequency. The frequency distribution can be determined by the frequency of data occurrence within each small range. Therefore, through CFD, the contribution rates of water from different sources can be more intuitively observed. At present, this method has been widely applied by scholars from various countries in the study of karst water systems (Guo *et al.* 2018).

Karst tidal springs, on the other hand, are sometimes stable and sometimes swollen due to their fluctuating flow (Guo *et al.* 2022a, 2022b), making their hydrological dynamics and sources more difficult to capture and quantify. Karst tidal springs refer to karst springs that are periodically discharged from groundwater under the control of special karst pipelines, also known as intermittent karst springs (Yang & Tan 1992), siphon springs (Sanz *et al.* 2016), periodic springs (Kansou & Bredeweg 2014), and rhythmic karst springs (Xiao & Zhang 2021). Karst siphon pipes are generally developed and are the decisive factor in the formation of karst tidal springs (Mudry *et al.* 2014). Intermittent upward conditions of the Earth's crust, easy development of dark rivers into cascade pipes (equivalent to dark river fractures), and a lack of branches are necessary conditions for the formation of tidal springs. Studies have proven (Dong 1983) that the cause of tidal springs is not the tidal influence of the Sun and Moon, but the siphoning of karst pipe flow. Zou (1993) successfully simulated the working principle of a karst groundwater siphon circulation zone through dynamic model tests.

The karst spring of Laolongshui in the underground river basin of Maocun, Guilin, Guangxi, China is a typical karst tidal spring (Wang 2005). Also, the dynamic change law of its springwater and its response to rainfall cannot be fully explored using hydrogeological surveys, tracer experiments, or geophysical exploration in the early stage. Hydrogeological surveys are commonly used to delineate groundwater types and clarify the composition of water bearing-rock formations (Quan & Yin 2023; Wang 2023); tracer experiments and geophysical exploration are mainly used to reveal the spatial structural characteristics of karst aquifer systems (Luan *et al.* 2021; Guo *et al.* 2022a, 2022b). Thus, there is room for improvement to explore the dynamics of the karst tidal spring. The goal of this study was to propose a faster and lower-cost method for the source investigation and dynamic change analysis of water resources in karst areas, especially for karst tidal springs. To achieve this goal, the specific objectives of this study are as follows: (1) a high-resolution observation of Laolongshui spring was set up to monitor the water level and electrical conductivity for two years to clarify the dynamic changes of the springwater. (2) The dynamic changes of springwater through 2 years of water level were clarified. (3) Through 2 years of automatic and continuous monitoring of electrical conductivity, the source of the components of the springwater in Laolongshui was determined using the frequency distribution of electrical conductivity. (4) Using CFD, the water mass contribution ratio of karst pipelines in the entire hydrological year was quantified under different rainfall intensities.

2. OVERVIEW OF THE RESEARCH AREA

Laolongshui is located in Shanwan Village, Lingchuan County, southeast of Guilin City, Guangxi, China, 30 km away from Guilin. It has a subtropical monsoon climate (Yang *et al.* 2012), and rainfall is mainly concentrated from April to August every year. There are four distinct seasons. Summers are hot and humid, and heavy rainfall is frequent; autumn rainfall decreases rapidly (Cao *et al.* 2011). The annual average temperature is 18.6 °C, and the annual rainfall amount is

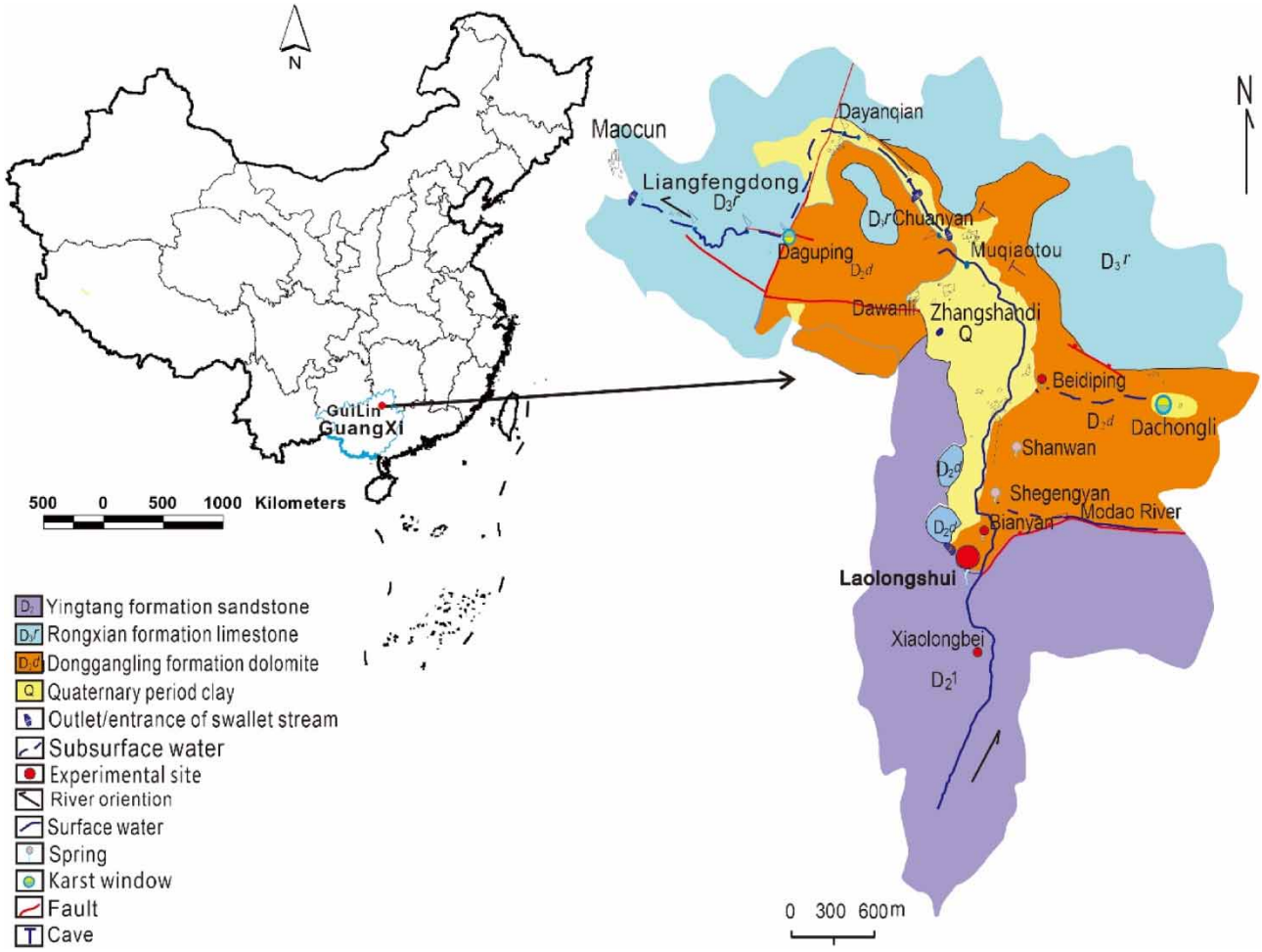

Figure 1 | Geological background map of the study area.

1,600–2,200 mm. Rainfall is affected by monsoon activity, and the spatial and temporal distributions are extremely uneven. Summer flooding and winter drought often occur.

Figure 1 shows that Laolongshui is located in the peak cluster depression of Maocun, with the bottom of the depression composed of Quaternary (Q) mud, gravel, and clay, which is the main area where residents live and work. The northern part of the depression is a karst area composed of pure limestone from the Upper Devonian Rongxian Formation (D_{3r}) and dolomite, limestone, and cloud limestone from the Middle Devonian Donggang Formation (D_{2d}), while the southern part is a non-karst area composed of clastic rock mixed with iron sandstone in the lower part of the Middle Devonian (D_2^1). Laolongshui is located on the intersection fault between the sand shale of the Yingtang Formation of the Middle Devonian and the limestone of the Donggangling Formation of the Middle Devonian, and springwater gushes out from the karst crevices of the gray-white clouds of the Donggangling Formation.

3. RESEARCH METHODS

3.1. High-resolution monitoring

The Laolongshui water level data were recorded using a HOBO U20L-04 automatic water level recorder, from ONSET, and the electrical conductivity data were obtained using a HOBO U24-002 electrical conductivity detector, made in the United States. The automatic monitoring interval was set to 15 min, and data acquisition and instrument calibration were carried out every month using the HOBO special software. For meteorological data collection, a HOBO U30 weather station, made in

the United States, was used to measure various parameters such as wind speed, wind direction, air temperature, humidity, total solar radiation, rainfall, and air pressure. The automatic sampling interval was set to 15 min.

3.2. On-site monitoring

For this study, on-site water quality analysis of the springwater in Laolongshui was conducted from August 2020 to July 2022. At the same time, the Beidiping karst spring (in the same basin's dolomite formation), Bianyan (receiving allogenic water), and the Xiaolongbei surface stream (in the clastic rock area) were compared, at intervals of generally 30 days. A total of 11 samples were taken. A French PONSEL portable water quality analyzer was used for on-site detection of the electrical conductivity, pH, and temperature of the water. At the same time, on-site detection of the $Ca^{2+}$and HCO_3^- content in springwater was carried out using a German Merck portable reagent kit. Water samples were collected in 600-ml polyethylene plastic bottles and sent to the laboratory of the Institute of Karst Geology, Chinese Academy of Geological Sciences. ICP-OES was used to detect the plasma concentrations of K^+, Na^+, Ca^{2+}, Mg^{2+}, Cl^-, SO_4^{2-}, and HCO_3^-, these seven ions are the most widely distributed in groundwater and largely determine the basic characteristics of groundwater chemistry. They are also the most important basis for distinguishing groundwater hydrochemical types.

3.3. Data analysis

CorelDraw2019, Origin2018, and Excel2016 were used for data plotting, processing, and statistical analysis. To obtain the saturation indices of calcite (SIc) and dolomite (SId), we used the WATSPEC program (Wigley 1977), which requires at least nine parameters: the water temperature, pH, and concentrations of seven major ions (Ca^{2+}, K^+, Na^+, Mg^{2+}, HCO_3^-, Cl^-, and SO_4^{2-}).

3.4. CFD decomposition method and principle

Assuming that the same type of water source has a normally distributed electrical conductivity, in addition, the electrical conductivity distribution of a single component of karst pipeline runoff is also normal without considering its source (Massei *et al.* 2007). CFD represents the superposition of electrical conductivity groups, which may include a combination of the overall electrical conductivity of two or more water groups (Guo *et al.* 2018). The CFD shape of a hydrological year approximates a histogram, and Origin2018's statistical program is used to find the probability density function that best corresponds to the histogram. Using Origin2018's peak fitting program, the probability density function is decomposed into its normally distributed component population. Using the residual method, all patterns or peaks that make up the original CFD are determined, including peak patterns that are not visible in the original curve. Since the basic distribution is normal, it is possible to determine the average and variance of the specific electrical conductivity of each water type determined through decomposition, as well as the proportion of that water type to the entire CFD. It is worth noting that because electrical conductivity is a reflection of ion charge rather than ion concentration unless the geochemical composition of different water types is similar, the proportion of CFD represented by each peak does not represent the volume proportion of the total flow formed by each peak. The proportion of peaks reflects the contribution rate of different water masses throughout the hydrological year. Laolongshui is a surface karst spring that is sensitive to precipitation and has significant differences in electrical conductivity. The peak ratios of various CFD peaks can reflect the contribution rate of water masses in karst pipelines under different rainfall intensities throughout the hydrological year.

4. RESULTS

4.1. Daily updates

The daily dynamic changes show that during the rainy season, the tidal increase is significant, and the maximum amplitude of water level change is 12.5 cm. Figure 2 shows that the water level rose 33 times within 24 h, indicating a tidal interval of 43.6 min. In addition, during rainstorms, the tidal phenomenon of the springwater level was temporarily affected. When the rainfall was reduced to a certain extent, the tide cycle of the springwater quickly recovered and became stable, and the tide cycle was no longer affected. Figure 2 shows that during the dry season, the fluctuation pattern of the springwater level is more pronounced, and the tidal period is significantly longer, at about 74–80 h. Additionally, the water level of the spring was relatively stable, with small tidal changes ranging from 3.5 to 4.3 cm.

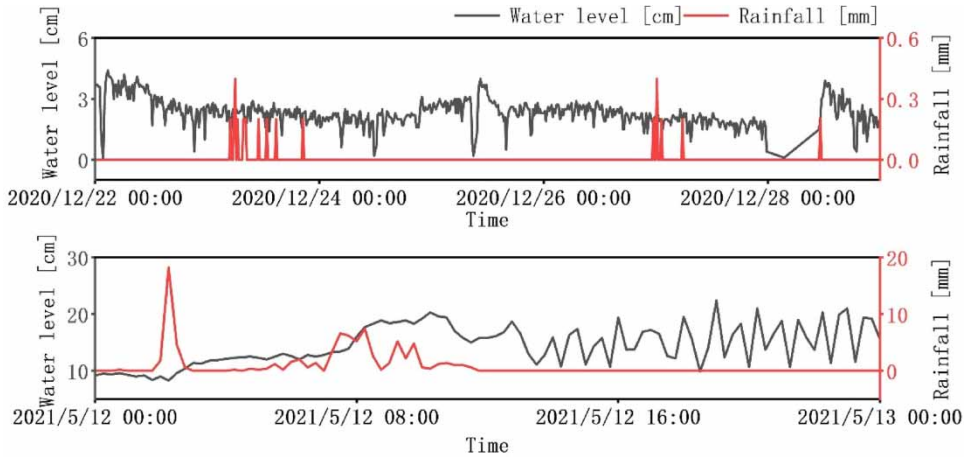

Figure 2 | Dynamic changes in the daily rainfall and water level.

4.2. Hydrochemical analysis

Beidiping is a karst spring originating from the dolomite area, with a maximum electrical conductivity of 533 μS/cm. Although Bianyan is located in the dolomite area, it has been supplied by allogenic water from upstream Xiaolongbei for a long period, with a maximum electrical conductivity of 228 μS/cm. The electrical conductivity of Xiaolongbei, located in the non-karst area upstream of Laolongshui, is generally between 11 and 57 μS/cm, while the electrical conductivity of rainwater in the study area is between 5.3 and 11.5 μS/cm. From Table 1, it can be seen that the variation characteristics of the

Table 1 | Hydrochemical comparison of springwater with different geological backgrounds and rainwater

Site name		EC μs/cm	SO_4^{2-} mg/L	Cl^- mg/L	HCO_3^- mg/L	K^+ mg/L	Na^+ mg/L	Mg^{2+} mg/L	Ca^{2+} mg/L	Sic	Sid
Laolongshui	Maximum	336.00	5.39	0.94	4.10	0.32	0.59	21.06	80.00	-1.70	-3.78
	Minimum	169.80	3.12	0.24	1.90	0.20	0.06	9.71	21.84	-2.44	-4.99
	Average	296.46	3.93	0.38	3.41	0.26	0.30	18.62	43.67	-2.20	-4.49
	Standard deviation	44.56	0.73	0.20	0.62	0.03	0.14	3.27	15.85	0.24	0.41
Beidiping	Maximum	533.00	10.66	1.63	6.00	0.72	0.54	15.16	122.00	-1.39	-3.55
	Minimum	330.00	3.05	0.61	4.00	0.23	0.11	9.03	70.21	-4.69	-5.10
	Average	462.56	4.94	1.00	5.23	0.46	0.41	12.16	90.49	-2.10	-4.31
	Standard deviation	63.14	2.34	0.32	0.71	0.18	0.12	2.26	14.97	0.89	0.46
Bianyan	Maximum	228.60	3.15	0.76	2.90	0.32	0.43	12.81	42.00	-2.37	-5.00
	Minimum	110.80	1.76	0.28	1.20	0.21	0.09	5.38	15.43	-3.76	-7.65
	Average	174.84	2.22	0.40	1.95	0.26	0.27	9.10	24.19	-2.90	-5.97
	Standard deviation	44.55	0.46	0.13	0.55	0.04	0.09	2.20	7.85	0.40	0.75
Xiaolongbei	Maximum	57.00	2.33	0.67	0.60	0.29	0.26	1.95	6.00	-4.26	-8.62
	Minimum	11.00	1.50	0.32	0.10	0.16	0.04	0.95	1.39	-5.53	-11.03
	Average	26.86	1.91	0.43	0.29	0.23	0.20	1.30	2.64	-4.92	-9.89
	Standard deviation	13.67	0.27	0.13	0.14	0.04	0.06	0.29	1.36	0.42	0.77
Rain	Maximum	11.50	2.67	1.13	0.10	1.14	0.08	3.38	1.79	-3.24	-7.00
	Minimum	5.30	0.48	0.18	0.00	0.17	-0.07	0.00	-0.00	-7.95	-15.34
	Average	8.10	1.19	0.38	0.02	0.43	-0.00	0.39	0.44	-5.91	-12.15
	Standard deviation	2.39	0.72	0.30	0.04	0.29	0.04	1.05	0.50	1.27	2.39

average electrical conductivity values of each spring and rainwater are as follows: Beidiping (462.56 μS/cm) > Laolongshui (296.46 μS/cm) > Bianyan (174.84 μS/cm) > Xiaolongbei (26.86 μS/cm) > Rain (8.10 μS/cm). The variation characteristics of the average HCO_3^- concentration are as follows: Beidiping (5.23 mg/L) > Laolongshui (3.41 mg/L) > Bianyan (1.95 mg/L) > Xiaolongbei (0.29 mg/L) > Rain (0.02 mg/L). The variation characteristics of the average Ca^{2+} concentration are as follows: Beidiping (90.49 mg/L) > Laolongshui (43.67 mg/L) > Bianyan (24.19 mg/L) > Xiaolongbei (2.64 mg/L) > Rain (0.44 mg/L). The variation characteristics of the average Mg^{2+} concentration are as follows: Laolongshui (18.62 mg/L) > Beidiping (12.16 mg/L) > Bianyan (9.10 mg/L) > Xiaolongbei (1.30 mg/L) > Rain (0.39 mg/L).

From Figure 3, it can be seen that the cation composition of Xiaolongbei is Ca^{2+} and Mg^{2+}, accounting for 28–7% and 19–37% of the total number of cations, respectively. The total proportion of $K^+ + Na^+$ has long exceeded 10%, reaching a maximum of 52%. The primary anion is HCO_3^-, accounting for 72–94% of the total number of anions. According to Schöeller's classification, Xiaolongbei's hydrochemical types are HCO_3-Ca-Mg, and HCO_3- (Na + Ca). The cations of Bianyan are mainly $Ca^{2+}$and Mg^{2+}, accounting for 68–81% and 18–30%, respectively, while HCO_3^- is the main anion, accounting for 97–98%. According to Schöeller's classification, the hydrochemical type of Bianyan is HCO_3-Ca-Mg. The main cations of Laolongshui are Ca^{2+} and Mg^{2+}, accounting for 65–81% and 19–34%, respectively, while the anion is HCO_3^-, accounting for 94–98%. According to Schöeller's classification, the hydrochemical type of Laolongshui is HCO_3-Ca-Mg. Bediping hydrochemistry mainly comprises Ca^{2+} and HCO_3^-, representing 85–91% cationic charge and 96–99% anionic charge, respectively.

4.3. Quantitative analysis of the CFD

Figure 4 shows that the decomposition results of the CFD for the two hydrological years are similar, both decomposed into four peaks, and the positions of each peak are relatively fixed. The proportions of each peak area from 2,020.8 to 2,021.7 are P1, 47.28; P2, 49.65; P3, 2.26; and P4, 0.81% (Table 2). The proportions of each peak area from 2,021.8 to 2,022.7 are P1,

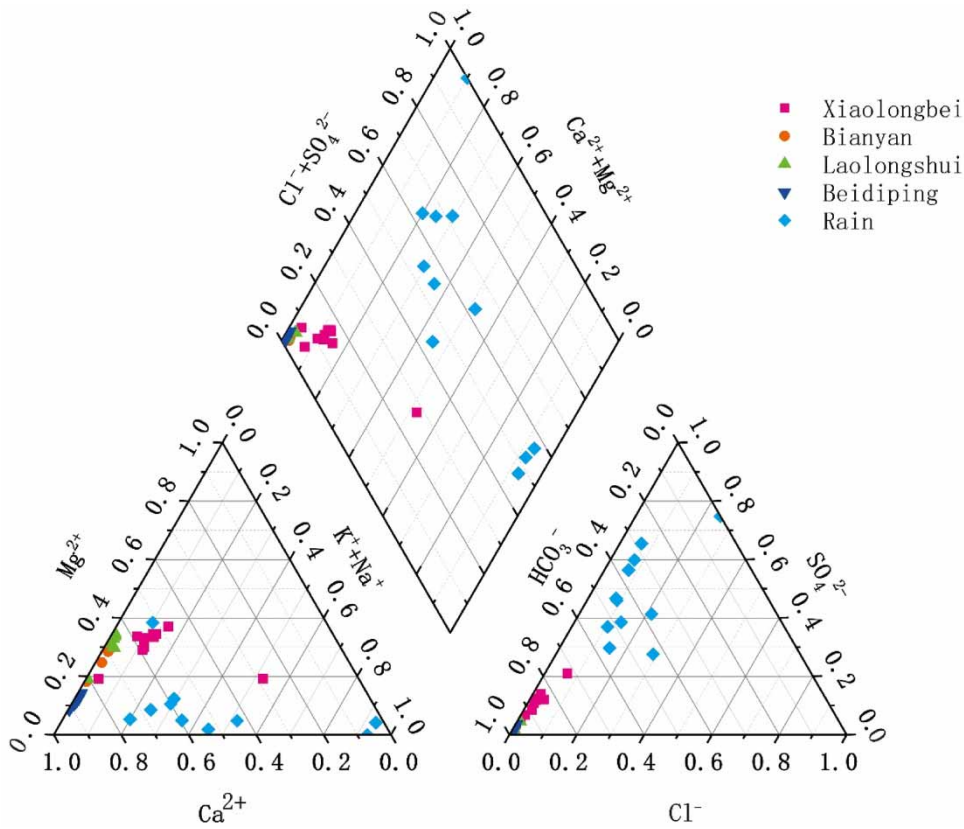

Figure 3 | Piper three-linear diagram of the hydrochemistry of springs in different geological backgrounds and rainwater.

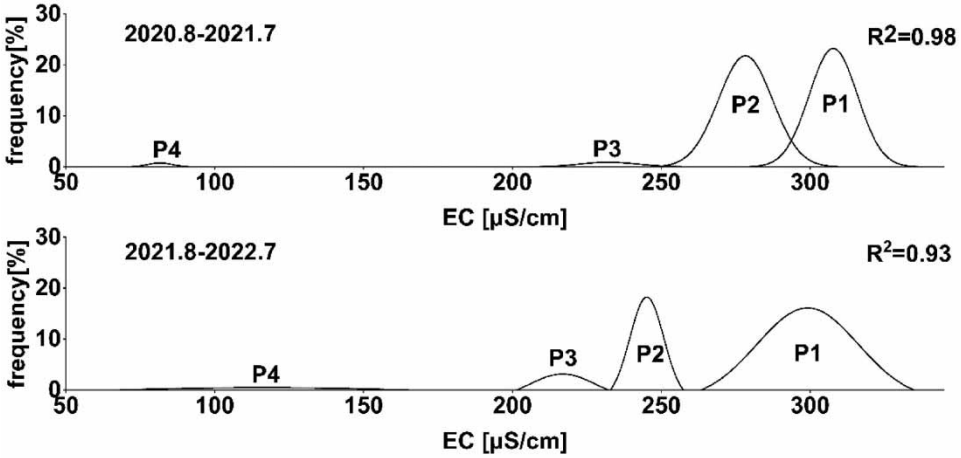

Figure 4 | CFD for Laolongshui.

Table 2 | Proportions of peak area, annual average flow, and total runoff

Year	P1	P2	P3	P4	Annual average flow (l/s)	Annual total runoff (100 million liters)
2020.8–2021.7	47.28%	49.65%	2.26%	0.81%	6.73	2.12
2021.8–2022.7	60.35%	28.93%	10.09%	0.62%	9.67	3.05
Average	53.82%	39.29%	6.18%	0.72%	8.20	2.58

60.35; P2, 28.93; P3, 10.09; and P4, 0.62%. There is a certain difference in the peak area of P2 between the two hydrological years, but overall, there is no significant difference in the position and trend of each peak.

Beidiping and Bianyan are located in the same Maocun underground river basin. One is a karst spring without an allogenic water supply (Jiang *et al.* 2012), and the other is a karst spring with a long-term allogenic water supply (Huang *et al.* 2011). In the CFD decomposition results of the two (Figure 5), there are significant differences in terms of the quantity and peak area. The CFD decomposition results for Beidiping are similar to those for Laolongshui, with the presence of isolated peaks and the isolated peaks having the smallest area. The electrical conductivity for the isolated peaks is also significantly lower than that

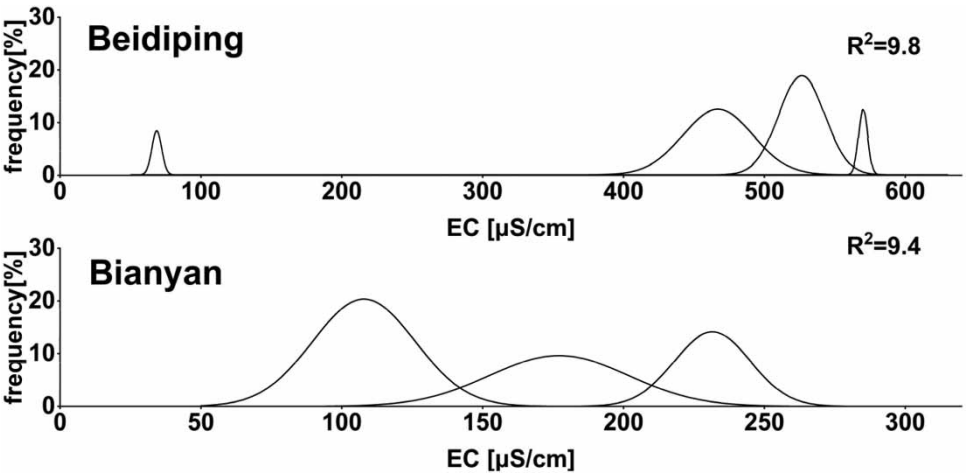

Figure 5 | CFD for Beidiping and Bianyan in 2021.

for the other three peaks. The CFD decomposition results for Bianyan show no isolated peaks, and the areas of the three peaks are equivalent. Overall, the three peaks decomposed from the CFD for Bianyan are relatively closely arranged and of relatively uniform size, and the overall electrical conductivity is much lower than that for Beidiping. The CFD decomposition results for Beidiping show diversity, with not only more peaks but also significant differences in the area of each peak.

4.4. Analysis of the causes of tidal springs

Zou (1993) demonstrated through model experiments the siphoning effect of multitidal springs and their unique karst groundwater dynamic characteristics. Figure 6 is a schematic diagram of the structure of a multitidal spring. A tide can only occur when the following three conditions are met: (1) H1 (the critical water level for siphoning in the reservoir) is equal to (or higher than) the elevation of point b; (2) h1 $<$ h2; and (3) Q1 $<$ Q2 or Q1 $<$ Q2 + Q3. Figure 7 shows the monitoring data from Laolongshui throughout the day, with a monitoring interval of 15 min. From Figure 7, it can be seen that the springwater rises once every 45 min, followed by an ebb tide. At high tide, the highest water level reaches 24.2 cm. At low tide, the lowest water level drops to 10.2 cm, giving a difference of 14 cm. In the case of intermittent replenishment during the rainy season, when the water level in the reservoir rises to H1, there is a siphon effect, with a rising tide followed by a falling tide. In this cycle, a tidal spring is formed, which is the hydrological and dynamic process of the Laolongshui tidal spring.

5. DISCUSSION

5.1. Analysis of water sources in tidal springs

Massei *et al.* (2007) analyzed four hydrological year data collected in Barton Springs, Austin, Texas, regarding the CFD and found that although the overall shape of CFD varies year by year, it can always be divided into the same group of normally distributed populations. Each population represents the type of water generated by a specific aquifer functional pattern.

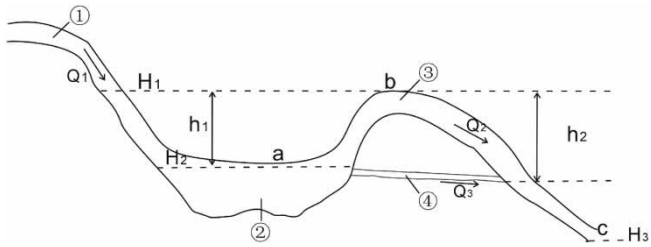

Figure 6 | Schematic diagram of the siphon structure (cited from (Zou 1993)). (1) The water supply pipeline, (2) relatively closed karst reservoir, (3) karst siphon pipeline, and (4) karst fissure lower than the siphon pipeline; H1 is the starting water level of the siphon and H2 is the stopping water level of the siphon; Q1, Q2, Q3, and Q4 are the flow rates during the operation of each pipeline; (a) is the lowest point at the inlet of the siphon, (b) is the highest point of the siphon, and (c) is the dew point of springwater, at the outlet of the siphon; h1 represents the height difference between points (a) and (b); and h2 represents the height difference between points (b) and (c).

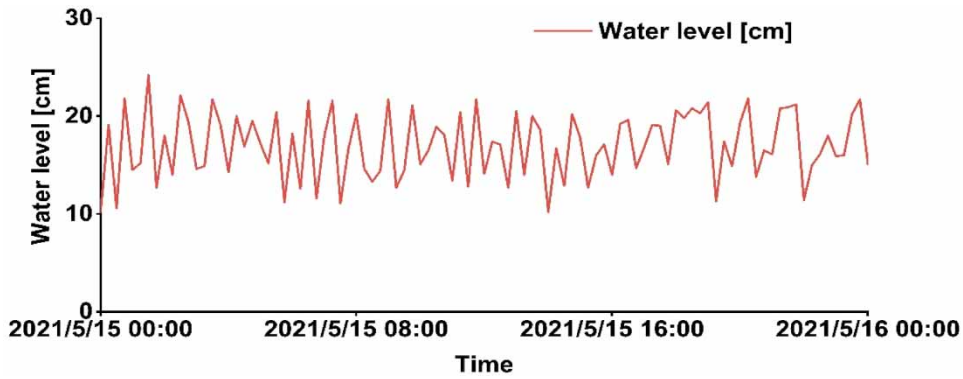

Figure 7 | Daily changes in the spring water level.

Therefore, to identify the proportions of water from different sources in springwater, the frequency distribution method in statistics is used to process electrical conductivity data. Guo *et al.* (2018) found through experiments that the decomposition results of CFD for four hydrological years at the same research point were similar, as they could all be decomposed into a series of similar peaks, indicating that the annual electrical conductivity distribution in the same region is roughly similar. The frequency distribution curve of electrical conductivity in Figure 6 shows four peaks, and the area of the peaks reflects the amount of electrical conductivity data within a certain range. The larger the peak, the greater the data volume, indicating a higher proportion from this water source. Each peak represents a water source that is influenced to varying degrees by factors such as the structure of the aquifer system, rainfall, and the intensity of water–rock interaction.

Previous studies have shown that Beidiping is a karst spring without an allogenic water supply (Huang *et al.* 2017). The CFD analysis results for Laolongshui and Beidiping are similar but differ significantly from those for Bianyan, which does have an allogenic water supply, indicating that the water supply mode of Laolongshui is the same as that of Beidiping. Meanwhile, the hydrochemistry of Laolongshui is closest to that of Beidiping, indicating that Laolongshui has no allogenic water supply. In addition, Huang *et al.* (2017) added tracers to Xiaolongbei upstream of Laolongshui but did not receive them in Laolongshui, which also confirmed this. Therefore, we believe that there are two main Laolongshui water source components: one is the water stored in the karst aquifer system, and the second is rainwater, which only arises from differences in seasonal rainfall, resulting in different degrees of dilution of springwater and different water–rock interaction times. Through comprehensive consideration of the hydrogeological background, rainfall, and upstream land use types in the Laolongshui area, we believe that P1 corresponds to the part where the water storage space inside the karst is slowly released during the dry season without rainfall. This part has a slow water flow rate and, after sufficient water–rock interaction has the highest electrical conductivity. The electrical conductivity of P2 is higher than that of P3 but lower than that of P1, indicating a prolonged and small amount of rainwater infiltration during the rainy season. The flow rate and velocity of this water are relatively small, and it has a smaller dilution effect on the internal karst water, so its electrical conductivity is also higher. P3 represents the high summer rainfall, when rainwater quickly infiltrates through the upper karst fissures, resulting in a high flow rate and a significant dilution effect on the water in the internal pipelines. Additionally, the water–rock interaction time is short, resulting in lower electrical conductivity. P4 represents the rapid infiltration of a large amount of rainwater within a short time during summer rainstorms. The internal water is diluted by a large amount of low-electrical conductivity rainwater within a short time, and the water–rock interaction time is very short, so the electrical conductivity of this part is the lowest. The electrical conductivity of the allogenic water from Xiaolongbei is the same (Table 1). Due to the short duration of rainfall at this level, the proportion of this water in the overall source is also the lowest. From the perspective of electrical conductivity values alone, it is easy to believe that this water is supplied by upstream allogenic water. However, by comparing its electrical conductivity distribution map and tracer experimental results, this source was excluded.

5.2. Analysis of the causes of wave peaks in the CFD curve

The electrical conductivity of groundwater is significantly influenced by karst hydrogeological conditions, which can comprehensively reflect the regional hydrodynamic conditions and lithological characteristics. The electrical conductivity of karst springwater flow has always been a fundamental variable for characterizing karst systems (Chang *et al.* 2021); it reflects the total amount of dissolved solids in the water. In karst water systems, dissolved solids are mainly controlled by the balance of calcium carbonate (Massei *et al.* 2007). Electrical conductivity reflects the degree of interaction between groundwater and rock, and its dynamic characteristics and distribution patterns are an important indicator (Smith *et al.* 2004). Changes in spring electrical conductivity provide information on local recharge and conduit flow in karst aquifers (Birk *et al.* 2004). The CFD curve can be decomposed into different peaks, which are determined by factors such as the pipeline size, the characteristics of each water source component, and the water area at the spring mouth (Guo *et al.* 2018). For example, the Lingshui Karst Spring in Nanning, Guangxi, has multiple water sources with significant electrical conductivity differences, and its CFD decomposes into four peaks without sufficient mixing. The Guancun underground river has a huge pipeline space, and its CFD has only one peak (Guo *et al.* 2018) because there are huge karst pipelines and caves upstream of the underground river with enough space to fully mix water from various sources (Huang *et al.* 2017). Similarly, Bianyan is the entrance where Xiaolongbei's surface water flows into the underground river in Maocun, mainly through fissure flow without sufficient mixing of various water sources. The spring area is equivalent to that of Laolongshui, but due to Bianyan's ability to continuously receive an allogenic supply with significant differences in electrical conductivity, its CFD is not as large as that for a karst spring with changes in rainfall and can only be decomposed into three peaks.

The electrical conductivity changes for Laolongshui and Beidiping are similar to those for Lingshui, with four peaks in the decomposition. The changes are mainly affected by rainfall, and the rainfall in the study area shows obvious seasonal characteristics. Therefore, the peaks decomposed from the Laolongshui CFD curve represent the degree of influence of different rainfall conditions on spring electrical conductivity.

6. CONCLUSION

Laolongshui is a typical karst tidal spring, and its hydrological process and formation are related to its unique geological structure. Through long-term monitoring, the dynamic changes of Laolongshui have been grasped, and the tidal patterns and causes have been clarified. This provides a certain data foundation for the development and utilization of groundwater resources and also has a certain significance for responding to geological disasters.

CFD is a more realistic and robust method for analyzing long-term electrical conductivity data, and it is easier to implement due to its low cost and ease of operation. The CFD of Laolongshui in two hydrological years has decomposed into four peaks (P1–P4), with significant differences in electrical conductivity values and peak positions, reflecting the degree of influence of different rainfall on water masses in karst pipelines. The source of the springwater in Laolongshui was quantified through CFD, mainly from the water stored in the karst aquifer system and rainwater. The electrical conductivity of the springwater is regulated by rainfall. Among the four peaks decomposed from the frequency distribution curve of electrical conductivity, P1 represents the slow release of water storage space inside the karst during the dry season without rainfall, and P2-P4 represents the dilution degree of springwater electrical conductivity or the duration of water rock interaction under different rainfall conditions. In addition, comparing the frequency distribution characteristics of the electrical conductivity of karst springs that receive and do not receive allogical water recharge in the same basin, it is confirmed that there is no allogenic water recharge in Laolongshui. This study found that CFD can effectively identify water masses with significant differences in karst water systems. This article suggests that this method can also help to identify the water source components of karst springs injected with different allogenic water sources.

ACKNOWLEDGEMENTS

This study was funded by National Natural Science Foundation of China (No. 2022YFF1300705, 42277077), Natural Science Foundation of Gunagxi (No. 2022GXNSFAA035569, Guike-AD21196005, 2021GXNSFBA075013), the Project of the China Geological Survey (No. DD20230547), and the Science and Technology Base and the Guilin Science Research and Technology Development Plan Project (2020010905).

DATA AVAILABILITY STATEMENT

All relevant data are included in the paper or its Supplementary Information.

CONFLICT OF INTEREST

The authors declare there is no conflict.

REFERENCES

Bakalowicz, M. 1979 *Contribution de la géochimie des eaux à la connaissance de l'aquifère karstique et de la karstification. Doctoral dissertation*, Laboratoire Souterrain du CNRS.

Birk, S., Liedl, R. & Sauter, M. 2004 Identification of localised recharge and conduit flow by combined analysis of hydraulic and physico-chemical spring responses (Urenbrunnen, SW-Germany). *Journal of Hydrology* **286**, 179–193. https://doi.org/10.1016/j.jhydrol.2003.09.007.

Cao, J., Yuan, D. & Pan, G. 2003 Some soil features in Karst Ecosystem. *Advances in Earth Science* **18** (1), 37–044.

Cao, J., Zhou, L., Yang, H., Lu, Q. & Kang, Z. 2011 Comparison of carbon transfer between forest soils in Karst and clasolite areas and the Karst carbon sink effect in Maocun village of GuiLin. *Quaternary Sciences* **31** (3), 431–437.

Chang, Y., Hartmann, A., Liu, L., Jiang, G. & Wu, J. 2021 Identifying more realistic model structures by electrical conductivity observations of the karst spring. *Water Resources Research* **57**, e2020WR028587. https://doi.org/10.1029/2020WR028587.

Chen, G. 2000 Study on the correlation between groundwater conductivity and total hardness. *Shandong Environment* **2000** (S1), 110–111.

Dar, F. A., Perrin, J., Ahmed, S. & Narayana, A. C. 2014 Review: Carbonate aquifers and future perspectives of karst hydrogeology in India. *Hydrogeol J* **22**, 1493–1506. https://doi.org/10.1007/s10040-014-1151-z.

Dong, X. 1983 A preliminary study on the genesis of karst tidal springs in southeast Sichuan. *Geology in China* **1983**, (8), 26–30.

Gao, F., Chen, S., Xing, D., Bian, X., Zhang, Z., A, A., Zhukovskaya, I. & Ershova, V. 2006 Analysis on correlation between characters of electric conductivity of groundwater and its main contaminant elements in Tieling area of Liaoning. *China World Geology* **25** (4), 424–428.

Goldscheider, N. & Drew, D. (Eds.) 2007 *Methods in Karst Hydrogeology*. Taylor & Francis, Leiden; New York.

Guo, F., Jiang, G., Liu, S. & Tang, Q. 2018 The frequency distribution of spring water conductivity was used to identify the water source components of karst aquifer system. *Advances in Water Science* **29** (2), 245–251.

Guo, X., Chen, Q., Huang, H., Wang, Z., Li, J., Huang, K. & Zhou, H. 2022a Water source identification and circulation characteristics of intermittent karst spring based on hydrochemistry and stable isotope – an example from Southern China. *Applied Geochemistry* **141**, 105309. https://doi.org/10.1016/j.apgeochem.2022.105309.

Guo, Y., Wu, P., Huang, F., Sun, P., Miao, Y. & Liu, S. 2022b Water flow characteristics of Maocun undergroun. *Carsologica Sinica* **41** (4), 577–587.

Hartmann, A., Goldscheider, N., Wagener, T., Lange, J. & Weiler, M. 2014 Karst water resources in a changing world: Review of hydrological modeling approaches. *Reviews of Geophysics* **52** (3), 218–242.

Hou, X. 2019 *Study on the Source of Spring Water Supply in Jinan*. University of Jinan.

Huang, F., Tang, W., Wang, J., Cao, J. & Yin, J. 2011 Effect of exogenous water on karst carbon sink —— take the underground river in Maocun in Guilin as an example. *Carsologica Sinica* **30** (4), 417–421.

Huang, F., Yin, W., Hu, X. & Cao, J. 2017 Quantitative tracing analysis of rainy season and dry season in the underground river basin of Maocun Village, Guilin. *Carsologica Sinica* **36** (5), 648–658.

Jiang, Z., Yuan, D., Cao, J., Qin, Q., He, S. & Zhang, C. 2012 A study of carbon sink capacity of karst processes in China. *Acta Geoscientica Sinica* **33** (2), 129–134.

Jiang, G., Guo, F. & Yu, S. 2015 Chemographs of Karst water system and its new application in hydrogeological survey. *Journal of Jilin University (Earth Science Edition)* **45** (3), 899–907.

Kansou, K. & Bredeweg, B. 2014 Hypothesis assessment with qualitative reasoning: Modelling the fontestorbes fountain. *Ecological Informatics* **19**, 71–89.

Luan, Z., Zhou, J. & Li, H. 2021 Exploring hidden structures in the Mohetai area using comprehensive geophysical methods. *Ground Water* **43** (6), 155–157 + 232.

Massei, N., Mahler, B. J., Bakalowicz, M., Fournier, M. & Dupont, J. P. 2007 Quantitative interpretation of specific conductance frequency distributions in karst. *Groundwater* **45**, 288–293. https://doi.org/10.1111/j.1745-6584.2006.00291.x.

Medici, G., Lorenzi, V., Sbarbati, C., Manetta, M. & Petitta, M. 2023 Structural classification, discharge statistics, and recession analysis from the springs of the Gran Sasso (Italy) carbonate aquifer; comparison with selected analogues worldwide. *Sustainability* **15** (13), 10125.

Moldovan, A., Hoaghia, M.-A., Kovacs, E., Mirea, I. C., Kenesz, M., Arghir, R. A., Petculescu, A., Levei, E. A. & Moldovan, O. T. 2020 Quality and health risk assessment associated with water consumption – a case study on karstic springs. *Water* **12**, 3510. https://doi.org/10.3390/w12123510.

Mudry, J., Zwahlen, F., Bertrand, C. & LaMoreaux, J. W. (Eds.) 2014 *H2Karst Research in Limestone Hydrogeology*. Springer International Publishing, Cham. https://doi.org/10.1007/978-3-319-06139-9.

Palmer, A. N. 2010 Understanding the hydrology of karst. *Geologia Croatica* **63** (2), 143–143.

Quan, Q. & Yin, L. 2023 Research on the importance of hydrogeological survey in the prevention of geological hazards in open pit mines. *China Metal Bulletin* **2023** (5), 165–167.

Richieri, B., Bittner, D., Hartmann, A., Benettin, P., Van Breukelen, B. M., Labat, D. & Chiogna, G. 2023 Using continuous electrical conductivity measurements to derive major solute concentrations in karst systems. *Hydrological Processes* **37**, e14929. https://doi.org/10.1002/hyp.14929.

Sanz, E., Rosas, P. & Menendez-Pidal, I. 2016 Drainage and siphoning of a karstic spring: A case study. *JCKS* **78**, 183–197. https://doi.org/10.4311/2015ES0134.

Smith, S. L., Whitaker, F. F., Parkes, R. J., Smart, P. L., Beddows, P. A. & Bottrell, S. H. 2004 The Geochemistry and Geomicrobiology of Saline Ground Waters: Yucatan Peninsula, Mexico. *Hydrogeology and Biology of Post-Paleozoic Carbonate Aquifers, Karst Waters Institute Special Publication* **7**, 135–137.

Vasić, L., Palcsu, L. & Fen, H. 2019 Groundwater gravitational circulation of Karst Veliko Vrelo and Malo Vrelo springs by isotope and the noble gas method: Case study of the Beljanica Massif. *Environmental Earth Sciences* **78**, 1–7.

Wang, J. 2005 *Study on Conductivity and NO3- Dynamics of the Outlet of Maocun Underground River in Guilin*. *Master's Dissertation*, Chinese Academy of Geological Science.

Wang, Z. 2023 Research on hydrogeological characteristics and prediction of mine pit water inflow in Tongshan Copper Mine. *Ground Water* **45** (3), 49–51.

Wang, G., Cheng, X. & Wu, G. 2008 Discussion on the formation mechanism and utilization restoration of karst spring-Taking Guizhou Province as an example. *Science & Technology Association Forum* **2008** (11), 59–60.

Wigley, T. M. L. 1977 WATSPEC-a computer program for determining the equilibrium of aqueous solutions. *British Geomorphology Research Group Technical Bulletin* **20**, 1–46.

Xiao, X. & Zhang, Q. 2021 Physical and analytical modeling of rhythmic karst springs. *JCKS* **83**, 109–119. https://doi.org/10.4311/2020ES0119.

Yang, M. & Tan, M. 1992 Dynamic model of intermittent siphon Karst spring. *Carsologica Sinica* **11** (2), 51–57.

Yang, H., Zhang, L., Yu, S. & Cao, J. 2012 Effects of different land – uses on the features of water-stable aggregates in karst and clasolite areas in Maocun, Guilin. *Carsologica Sinica* **31** (3), 265–271.

Yu, B., Xiao, M., Wang, X. & Fei, X. 2020 Study on the dynamic changes of spring flow, conductivity and pH value. *Geology and Resources* **29** (4), 380–387.

Zhang, Z., Xu, Y., Zhang, Y. & Cao, J. 2019 Review: Karst springs in Shanxi, China. *Carbonates Evaporites* **34**, 1213–1240. https://doi.org/10.1007/s13146-018-0440-3.

Zhou, R. & Li, Y. 2022 Springs can perceive earthquakes. *Bulletin of Mineralogy, Petrology and Geochemistry* **41** (2), 461–464. doi:10.19658/j.issn.1007-2802.2022.41.040.

Zou, C. 1993 Study on the development law of karst multi-tide springs. *Carsologica Sinica* **12** (2), 40–48.

First received 10 November 2023; accepted in revised form 29 January 2024. Available online 14 February 2024